Available online at www.sciencedirect.com
ScienceDirect
European Polymer Journal 43 (2007) 3236–3249
EUROPEAN POLYMER JOURNAL
www.elsevier.com/locate/europolj

Macromolecular Nanotechnology

Incorporation of hydrodynamic interaction forces to molecular statistical theory of temporary polymer networks in solution

Dimitrios Chassapis [a,*], Thodoris D. Karapantsios [b], Anastasios Balouktsis [c]

[a] Department of Mechanical Engineering, Technological Education Institute of Serres, End of Magnesia's str., GR-62100 Serres, Greece
[b] Department of Chemistry, Chemical Technology Division, Aristotle University of Thessaloniki, Box 116, GR-54124 Thessaloniki, Greece
[c] Department of Information and Communications, Technological Education Institute of Serres, End of Magnesia's str., GR-62100 Serres, Greece

Received 3 August 2006; received in revised form 20 April 2007; accepted 27 April 2007
Available online 22 May 2007

Abstract

Molecular statistical theory of temporary polymer networks is an integrated approach to describe the rheological behavior of such networks based on information at a molecular level. Predictions of the theory regarding the dependence of viscometric functions on shear rate in stationary shear flow are at satisfactory accord with measurements. However, due to the exceeding complexity of the descriptive equations, their formulation and assessment has been performed so far only for cases where hydrodynamic interaction is negligible. In the present work, this effect is included in the model equations through the Oseen tensor. Incorporating the hydrodynamic interaction for the case of simple shear flow of two different polystyrene solutions, leads to theoretical results that agree a little better with experimental values, in terms of viscometric functions. Moreover, a non-zero negative value of the second normal-stress difference is predicted. For the case of elongation flow of the same polystyrene solutions there are no experimental results to compare with, so the appraisal of the theory was based solely on the reasonable dependence of the computed elongation viscosity on elongation rate.

Keywords: Temporary polymer networks; Hydrodynamic interaction; Viscometric functions; Oseen tensor

1. Introduction

It is rather a common consensus in the scientific community that the rheology of concentrated polymer solutions and polymer melts is based on the idea of the reptation motion of a macromolecule [1] confined in a tube-like region made of the surrounding chains [2]. Because of the weakness of the original Doi–Edwards reptation-tube theory [2] to describe the phenomenon of viscoelasticity, modern reptation-tube models incorporate several improvements such us chain-length fluctuations [3–5] subchain stretching [6–9], double reptation [10–12], convective constraint release [13,14].

The progress achieved by recent models, numerical or analytical, is substantial since they manage

* Corresponding author. Fax: +30 23210 46556.
E-mail address: dcasap@teiser.gr (D. Chassapis).

0014-3057/$ - see front matter © 2007 Elsevier Ltd. All rights reserved.
doi:10.1016/j.eurpolymj.2007.04.041

to describe quantitatively most experimental rheological data with the help of a small set of material specific parameters such as the tube diameter, the plateau modulus and the elastic modulus. Nevertheless, these parameters have often to be deduced from experiments in the non-Newtonian range [15] where, in principle, we have not reached yet the point of a consistent interpretation concerning the behavior of entangled polymers [16]. Furthermore, it seems that the reptation mechanism dominates in cases of strong entangled polymers with more than ten entanglements per macromolecule [17]. It is this reason that made us reappraise an older molecular statistical theory approach [18] to describe semi-dilute polymer solutions. The present work is in the tradition of bead–spring models of dilute solutions but modified to describe semi-dilute solutions of weakly entangled polymers (2–10 entanglements per macromolecule) by adding a creation/decay term for temporary network junctions. Several variations of the temporary network model have been communicated in literature improving different aspects of the analysis each time [19]. Among those that have found broad acceptance, special attention should be given to the *Multimode Giesekus* [20] and *Phan-Thien Tanner (PTT)* [21] models which were meant to describe semi-dilute to lightly entangled polymer solutions and therefore have relevance to this work. The multimode Giesekus model achieves excellent fits of shear flow data but not so good fits of elongational flow data [19,22,23]. On the other hand, the PTT model gives excellent fits of either shear or elongational flow data, but not of both of them simultaneously [19,22,23]. In addition, in complex kinematic flows such as planar entry flows and flows past a cylinder both models are capable of providing quantitative predictions only over a limited range of Weissenberg numbers (i.e. $We = \lambda\kappa$ where λ is the mean relaxation time of the test fluid and κ is a characteristic strain rate in the flow) [24–26]. Moreover, these models treat polymer flows in a rather phenomenological manner which does not clarify the physics of the elementary kinetic processes on a molecular level. Despite the above shortcomings, it is evident that the temporary network model has strong potential. It is hoped that after further development this approach may offer a tempting alternative in situations that other theories fail.

The junctions of a temporary polymer network have by definition the capability to decay and form. Therefore, such a network presents increased mobility, compared to a permanent network, which is macroscopically manifested as viscoelasticity. In order to estimate the corresponding non-Newtonian material functions, Kroener and Takserman-Krozer [18] developed a molecular statistical theory of temporary polymer networks in solution, in the framework of a generalized spring–bead model, in which springs represent network chains whereas their beads stand for the non-permanent bonds. A schematic of the network model is shown in Fig. 1.

A chief point of the Kroener and Krozer theory is the transformation of the generalized Kirkwood diffusion equation from a high dimensional integro-differential equation to a high dimensional differential equation. This simplification is achieved through the relaxation time approach [18], due to which the diffusion equation takes the following form

$$\frac{\partial W}{\partial t} + \sum_{i}^{M} \vec{\nabla}_i \cdot (\dot{\vec{r}}_i W) = -\bar{p}(W - W_{\mathrm{eq}}) \tag{1}$$

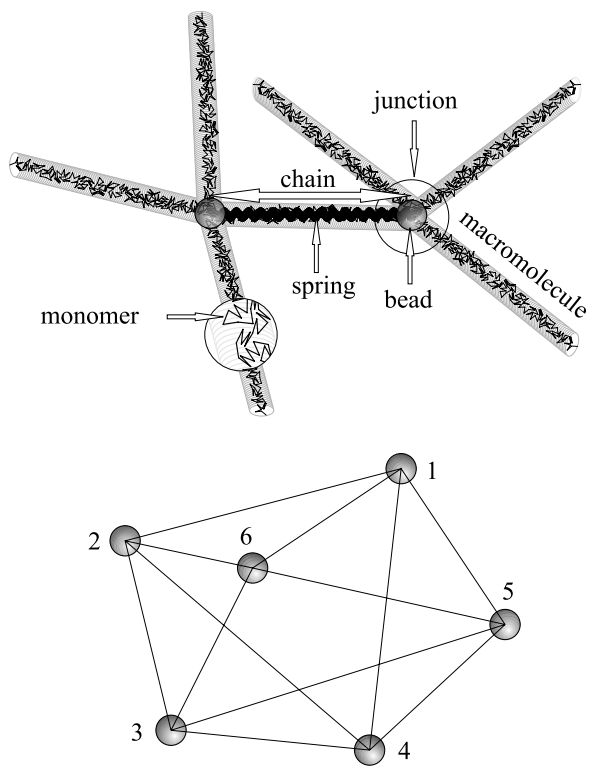

Fig. 1. Schematic of the network model. The top picture shows the relation between the "actual" molecular structure, the chains, the junctions, the beads and the springs. The bottom picture shows a four-functional network model with $M = 6$. For simplicity, the bead distances h_{ij} are shown instead of the complex macromolecular chains.

where

- $W = W(\vec{R}, Z, M, t)$ is the non-equilibrium probability density function for the state $[\vec{R}, Z, M]$ at time t.
- $\vec{R} = \{\vec{r}_i\}$ $(i = 1, 2, \ldots, M)$ is the configurational position vector for the beads. $Z = \{z_{ij}\}$ is the set of numbers z_{ij}, which denotes how many monomers form the chain by connecting the neighboring junctions i and j.
- M is the number of beads per volume V. In the model (four-functional network without open ends) there are M junctions and $2M$ chains connecting them.
- $\vec{\nabla}_i$ is the Nabla operator belonging to $\vec{r}_i$.
- W_{eq} is the equilibrium probability density function. It must be mentioned that within the relaxation time approach [18] $W(Z) = W_{\text{eq}}(Z)$. We expect that this is a good approximation as long as the velocity gradient is not too large.
- $\dot{\vec{r}}_i$ is the velocity of the ith bead.
- $\bar{p} = \bar{p}(\vec{R}, Z) \equiv \int\int p(\vec{R}, Z \to \vec{R}', Z')\mathrm{d}\vec{R}'\mathrm{d}Z'$ is the probability per unit time that the configuration $(\vec{R}, Z)$ will decay into any other configuration. This was calculated [18] under the assumption that (i) the density of decay processes is not too high in time and space and (ii) $\bar{p}(\vec{R}, Z)$ and $h_{ij} \equiv |\vec{r}_j - \vec{r}_i|$ can be replaced by $\bar{p}(\langle\vec{R}\rangle_R, Z)$ and $\langle h_{ij}\rangle$ respectively, where the brackets $\langle\,\rangle$ denote ensemble average. The result is given in Appendix A.

The velocities of the beads obey a Langevin-type equation (see next section), whose form is determined by the forces acting on the beads. In the past, the forces that have been included in the Langevin equation for the assessment of the molecular statistical theory of temporary polymer networks were elastic forces (transmitted through the chains), frictional forces between polymer and solvent and statistical entropy forces of Brownian motion [18,27–30].

In this work, we shall make a step ahead by incorporating hydrodynamic interaction forces in the model equations. It is recognized that hydrodynamic interactions are expected to be less relevant in more concentrated systems than in dilute solutions. Moreover, the concept of blobs and screening in a multiscale approach, e.g. [31,32], suggests that hydrodynamic interactions should be screened on the mesh scale of the network (up to the mesh scale they are described by the solvent viscosity). However, the present molecular statistical model aims to describe semi-dilute solutions of weakly entangled polymers (2–10 entanglements per macromolecule) where it is presently unclear whether hydrodynamic interactions may play a role under conditions of practical interest. For this reason, predictions based on the new model equations will be compared against experimental results for semi-dilute solutions from literature. To the best of our knowledge, this is the first time that hydrodynamic interaction forces are included in the molecular statistical theory of temporary polymer networks.

2. Langevin-type diffusion equation with hydrodynamic interaction

In formulating the equations of motion for the beads it is assumed that inertial forces can be ignored. This approximation is rather common when using the spring–bead model [33,34]. In addition to the forces employed in earlier studies acting on the beads of the molecular statistical theory of temporary polymer networks (mentioned above), here hydrodynamic interaction forces are also involved. It is still left for the future to study the forces of the excluded volume effect. To this end, the Langevin-type equation takes the form

$$\dot{\vec{r}}_i = \vec{r}_i \cdot \vec{\nabla}\vec{u} - \frac{1}{\zeta}\sum_j^M \kappa_{ij}\vec{r}_j - D\vec{\nabla}_i \ln W - \sum_j^M \underline{\underline{\Omega}}_{ij} \cdot \left(\sum_l^M \kappa_{jl}\vec{r}_l + k_{\text{B}}T\vec{\nabla}_j \ln W\right) \tag{2}$$

where the dot denotes the scalar multiplication.

The other mathematical symbols are explained as follows:

- $\vec{u}$ is the fluid velocity.
- ζ is the effective friction constant, which accounts not only for the friction between polymer and solvent but also for the friction between macromolecular chains that come in contact. This constant is an experimentally determined parameter [18,27].
- (κ_{ij}) is the elasticity matrix, which is associated with the matrix (k_{ij}) of the spring constants of chains (ij) through the following relations [27]

$$\kappa_{ij} = \sum_j^M k_{ij}\ (i = j), \quad \kappa_{ij} = -k_{ij}\ (i \neq j) \tag{3}$$

For a linearized elasticity, the spring constants k_{ij} are given from a known formula of Volkenstein [35] and Flory [36].

- $D = \frac{k_B T}{\zeta}$ is the diffusion constant, k_B is Boltzmann's constant and T is the absolute temperature.
- $\underline{\underline{\Omega}}_{ij}$ is the Oseen tensor, which describes the hydrodynamic interaction between beads i and j, and is given as

$$\underline{\underline{\Omega}}_{ij} = \begin{cases} \frac{1}{8\pi\eta_{ef} h_{ij}} \left(\underline{\underline{1}} + \frac{\vec{h}_{ij}\vec{h}_{ij}}{h_{ij}^2} \right) & \text{for } i \neq j \\ 0, & \text{for } i = j \end{cases} \quad (4)$$

where $\underline{\underline{1}}$ is the (three-dimensional) unit tensor and η_{ef} is the effective viscosity of the polymer solution, as deduced from the Stokes expression: $\zeta = 6\pi\eta_{ef} R_B$, where $R_B = \left(\frac{3M_{mon}L}{\pi M N_A \rho}\right)^{1/3}$ is the radius of (spherical) beads.

M_{mon} is the molecular weight of the monomer, L is the number of monomers in the network system with M beads and $2M$ chains, N_A is the Avogadro–Loschmidt number and ρ is the polymer density. L and ζ are parameters that must be obtained experimentally.

Along with L and ζ, there is yet a third parameter which must be determined experimentally in order to solve the model equations. This is v^* (a frequency parameter whose significance is explained in Section 4) [18,27]. Thus, we have a theory with three adjustable parameters which holds already before incorporating the hydrodynamic interaction. Nevertheless, it is noteworthy that these parameters are determined from experiments in the Newtonian range, so that predictions about the non-Newtonian regime are indeed predictions. The same holds for elongational flow for which it is not necessary to determine any parameter either in the Newtonian or the non-Newtonian range.

The use of the effective viscosity η_{ef} of the polymer solution and not of just the viscosity of the solvent, as customary done for dilute polymer solutions, is because ζ (as it is calculated; see Appendix A) accounts also for the friction between polymer units coming in contact. In this way, the screening effect of network chains with regards the hydrodynamic interaction of beads is taken into account. Thus, we use an effective Oseen tensor, in the same way we use an effective friction constant. The effective viscosity η_{ef} is used also for computing the hydrodynamic interaction parameter $h^* = (\zeta/\eta_{ef})[k/(36\pi^3 k_B T)]^{1/2}$ (where k is the mean spring constant).

3. Stress tensor and second moments

The stress tensor $\underline{\underline{\pi}}$ of the network, which is the base from which all material functions are computed, is given according to Giesekus [19, Chapter 13] from the relation [27]:

$$\underline{\underline{\pi}} = \frac{N_A c}{M_{pol}} \sum_{i'}^{M} \lambda_{i'} \langle \vec{s}_{i'} \vec{s}_{i'} \rangle_S \quad (5)$$

Here

- c is the mass concentration of the polymer.
- M_{pol} is the molecular weight of the polymer.
- $\vec{s}_{i'}$ are the eigenvectors belonging to the vibrating system of beads and the elastic springs among them. We use the subscripts i' instead of i, because they signify modes and not beads.
- $\lambda_{i'}$ are the eigenvalues of the elastic matrix (κ_{ij}).
- $\langle \vec{s}_{i'} \vec{s}_{i'} \rangle_S$ are the so-called second moments in the mode representation of the vibrating molecular network. Index "s" designates an ensemble average with respect to the entire mode space $\vec{S} = \{\vec{s}_{i'}\}$.

To calculate the stress tensor one needs to know these second moments. Their calculation can be performed by a standard procedure from the diffusion equation, after this equation is transformed to normal modes. This methodology, employed also by Kroener and Takserman-Krozer [18] and Chassapis [27], leads to the following expression

$$\frac{\partial}{\partial t} \langle \vec{s}_{i'} \vec{s}_{i'} \rangle_S - \underline{\underline{\beta}}_{i'} \cdot \langle \vec{s}_{i'} \vec{s}_{i'} \rangle_S - \langle \vec{s}_{i'} \vec{s}_{i'} \rangle_S \cdot \underline{\underline{\beta}}_{i'}^{\dagger} = 2\underline{\underline{\varepsilon}}_{i'} \quad (6)$$

With $\underline{\underline{\beta}}^{\dagger}$ being the transpose of $\underline{\underline{\beta}}_{i'}$ and

$$\underline{\underline{\beta}}_{i'} = (\vec{\nabla}\vec{u})^{\dagger} - \left[\frac{\bar{p}}{2} + \frac{\lambda_{i'}}{\zeta} \right] \underline{\underline{1}} - \underline{\underline{A}}_{i'},$$

$$\underline{\underline{\varepsilon}}_{i'} = \frac{\bar{p}}{2} \langle \vec{s}_{i'} \vec{s}_{i'} \rangle_{Seq} + D\underline{\underline{1}} + k_B T \underline{\underline{B}}_{i'} \quad (7)$$

In the above, $(\vec{\nabla}\vec{u})^{\dagger}$ is the transpose of the velocity gradient tensor $\vec{\nabla}\vec{u}$ and

$$\underline{\underline{A}}_{i'} = \sum_{i}^{M} \sum_{j}^{M} \sum_{l}^{M} q_{ii'} q_{li'} \kappa_{jl} \underline{\underline{\Omega}}_{ij},$$

$$\underline{\underline{B}}_{i'} = \sum_{i}^{M} \sum_{j}^{M} q_{ii'} q_{ji'} \underline{\underline{\Omega}}_{ij} \quad (8)$$

In Eq. (8), $q_{ii'}$ is the ith component of the i'th eigenvector of the elasticity matrix (κ_{ij}) introduced in Section 2.

The value of second moments at *equilibrium* ($\vec{\nabla}\vec{u} \to 0$) is derived from Eq. (6):

$$\langle \vec{s}_{i'}\vec{s}_{i'}\rangle_{\mathrm{Seq}} = \frac{k_{\mathrm{B}}T}{\lambda_{i'}}\underline{\underline{1}} \tag{9}$$

This value is exactly the same as in previous studies [27]. Apparently, the present Eq. (6) for calculating the second moments is compatible with the respective earlier one, which did not consider hydrodynamic interaction forces [18,27–30].

Eq. (6) was derived under the assumptions:

1. $\underline{\underline{\Omega}}_{ij}$ does not depend on $\vec{S}$ and thus also not on $\vec{R}$. Without this assumption the second moments can only be determined if the whole distribution function is known. In order to avoid this complication, we replace $\underline{\underline{\Omega}}_{ij}(\vec{R})$ by $\underline{\underline{\Omega}}_{ij}(\langle\vec{R}\rangle)$ similar to the variable substitution performed for the estimation of $\overline{p}$ in Eq. (1).
2. $\langle \vec{s}_{i'}\vec{s}_{j'}\rangle_S = \langle \vec{s}_{i'}\vec{s}_{j'}\rangle_S \delta_{i'j'}$. This equality holds rigorously in the case that hydrodynamic interaction is negligible, so we expect this to be a reasonable approximation since the relaxation time approach based on which the diffusion Eq. (1) was derived is valid only when the z-distribution is close to its equilibrium value [18], i.e. for not too large velocity gradients. The effect of relaxing this assumption is the subject of a subsequent publication.

After that the Oseen tensor in mode representation for simple shear and elongational flow is given by (superscripts denote the Cartesian tensor components)

$$\underline{\underline{\Omega}}_{ij}^{kl} = \frac{1}{8\pi\eta_{\mathrm{ef}}}\left\{\frac{1}{\left(\sum_{i'}^{M}(q_{ji'}-q_{ii'})^2\langle(s_{i'})^2\rangle_S\right)^{1/2}} \times\left[\underline{\underline{1}} + (-1)^{(1-\delta_{kl})}\frac{\sum_{i'}^{M}(q_{ji'}-q_{ii'})^2\langle\vec{s}_{i'}\vec{s}_{i'}\rangle_S^{kl}}{\sum_{i'}^{M}(q_{ji'}-q_{ii'})^2\langle(s_{i'})^2\rangle_S}\right]\right\} \tag{10}$$

The factor $(-1)^{(1-\delta_{kl})}$ takes into account that the above substitution of $\underline{\underline{\Omega}}_{ij}(\vec{R})$ by $\underline{\underline{\Omega}}_{jj}(\langle\vec{R}\rangle)$ changes the sign of the non-vanishing non-diagonal Oseen tensor components in simple shear flow, as obtained after some elementary geometrical analysis (see Appendix B). In Eq. (10), $\langle(s_{i'})^2\rangle$ is the trace of $\langle \vec{s}_{i'}\vec{s}_{i'}\rangle$.

3.1. Shear and elongational flow

In the case of simple shear and elongational flow, the velocity gradient tensor has the following form in Cartesian coordinates:

$$\vec{\nabla}\vec{u} = \dot{\gamma}\begin{pmatrix}0&0&0\\1&0&0\\0&0&0\end{pmatrix}, \quad \vec{\nabla}\vec{u} = \dot{\varepsilon}\begin{pmatrix}-\frac{1}{2}&0&0\\0&-\frac{1}{2}&0\\0&0&1\end{pmatrix} \tag{11}$$

$\dot{\gamma}$ and $\dot{\varepsilon}$ is the constant shear and elongation rate respectively.

The viscometric functions that are of interest in the case of elongational and simple shear flow are the viscosity function $\eta(\dot{\gamma})$, the first and second normal-stress difference $\Psi_1(\dot{\gamma})$, $\Psi_2(\dot{\gamma})$ and the elongational viscosity function $\eta_{\mathrm{e}}(\dot{\varepsilon})$. They are defined as follows:

$$\eta(\dot{\gamma}) = \frac{\pi^{21}}{\dot{\gamma}^2}, \quad \Psi_1(\dot{\gamma}) = \frac{\pi^{11}-\pi^{22}}{\dot{\gamma}^2},$$
$$\Psi_2(\dot{\gamma}) = \frac{\pi^{22}-\pi^{33}}{\dot{\gamma}^2}, \quad \eta_{\mathrm{e}}(\dot{\varepsilon}) = \frac{\pi^{33}-\pi^{11}}{\dot{\varepsilon}} \tag{12}$$

From Eq. (6) one can calculate the components of $\langle \vec{s}_{i'}\vec{s}_{i'}\rangle_S$, that are needed for the calculation of the viscometric functions. At this point, the following must be stressed. The transition probability is a function of the trace $\langle(s_{i'})^2\rangle$ [18]. Yet, the trace itself is a function of the transition probability. Furthermore, the effective Oseen tensor is a function of the second moments and vice versa. These features turn the above equations into transcendental requiring a numerical evaluation, which, however, does not present particular difficulties to solve. Once the value of the trace $\langle(s_{i'})^2\rangle_S$ is estimated, the computation of the mean distance of two arbitrary beads, h, is straightforward from the relation:

$$h = \frac{1}{M(M-1)}\sum_{i=1}^{M}\sum_{j=1}^{M}\langle h_{ij}\rangle_S = \frac{1}{M(M-1)}\sum_{i=1}^{M}\sum_{j=1}^{M}\left(\sum_{i'}^{M}(q_j^{i'}-q_i^{i'})^2\langle(s_{i'})^2\rangle_S\right)^{1/2} \tag{13}$$

4. Results and discussion

The aforementioned viscometric functions are calculated for two different solutions of polystyrene from literature [22,37] for the cases of simple shear

flow and elongational flow. As it is explained in Appendix A, the calculation of the viscometric functions requires the *simultaneous* knowledge of the limiting parameters $\eta_0 = \lim_{\dot{\gamma}\to 0}\eta$ and $\Psi_{10} = \lim_{\dot{\gamma}\to 0}\Psi_1$ for shear flow. This requirement greatly diminishes the extent of usable published experimental data to compare with. The selected two polystyrene solutions fulfil these conditions. The specific parameters of these solutions are displayed in Table 1.

The calculation of the second moments, from which the viscometric functions are computed, requires the diagonalization of the $(M \times M)$ elastic matrix. In the present calculation, a value of $M = 20$ is employed, making a compromise between accuracy and computational effort. For instance, increasing M from 10 to 15 varies the viscometric functions η, Ψ_1, Ψ_2 and η_e by 0.15%, 0.25%, 35% and 0.7%, respectively, while it rises the CPU time from 6.7 min to 14.2 min. However, for a further increase of M from 15 to 20 the corresponding variations are only 0.01%, 0.01%, 5% and 0.1%, whereas the CPU time becomes 27 min. Table 2 presents a few calculated parameters of both polymer solutions.

As can be seen in Table 2, the incorporation of hydrodynamic interaction in the model equations results in a considerable reduction of the predicted effective friction constant ζ(≈22% for both solutions). Apparently, the larger $\zeta_{w/oHI}$ (effective friction constant without hydrodynamic interaction) values, are in error since they attribute part of the resistance of the beads (that due to hydrodynamic interactions) to a friction contribution. At the same table, one can further notice that accounting for hydrodynamic interaction produces appreciably lower values of the parameter v^*, which determines the stability of beads (see Appendix A). Yet, this reduction is quite different between the two solutions; 8.4% and 17.2%, respectively.

It must be noted here that the calculated values of the hydrodynamic interaction parameter h^* agree fully with those that have been used in studying polystyrene solutions by Johnson et al. [38], Prakash and Öttinger [39] and Chih-Chen Hsieh et al. [40].

4.1. Mean bead distance and transition probability

Hydrodynamic interaction is responsible only for a minor increase of the mean distance between arbitrary beads from $h_{w/oHI}$ to h, Fig. 4. The increase is not observable in the Newtonian range (low $\dot{\gamma}$ or $\dot{\varepsilon}$). Then it reaches a maximum at the beginning of the non-Newtonian range. And finally, it decays gradually as the velocity gradient rises even further. The behavior in the Newtonian range is accredited to the isotropy of Oseen tensor at small velocity gradients e.g. Fig. 2. The decay at large velocity gradients is the result of a progressive weakening of hydrodynamic interaction caused by the increasing mean bead distance h as $\dot{\gamma}$ or $\dot{\varepsilon}$ increases, Fig. 3.

Nevertheless, the most profound effect of hydrodynamic interaction is not in altering the mean bead distance but in modifying the transition probability, in other words the stability, of the beads. This is shown in Fig. 6 where the ratio $p/p_{w/oHI}$ is plotted against the shear or elongation rate for both polymer solutions. As with h and p without a subscript denotes the situation with hydrodynamic interaction whereas $p_{w/oHI}$ the one without it. Evidently, the incorporation of hydrodynamic interaction reduces the transition probability appreciably and as a consequence increases the stability of beads.

Table 1
Parameters of the polymer solutions

Polymer solution		c (kg/m^3)	$M_{pol} \times 10^{-6}$	Θ (°C)	η_0 (Pa s)	ξ_0 (Pa s^2)
A	Polystyrene in toluene [37]	125	1.86	25	31.5	5.5
B	Polystyrene in a mixture of tricresyl phosphate and dioctyl phthalate [22]	51.75	1.92	22	35.5	20

c is the mass concentration of the polymer, M_{pol} is the molecular weight of the polymer and Θ is the temperature.

Table 2
Calculated parameters of the polymer solutions

Polymer solution	$\zeta \leftrightarrow \zeta_{w/oHI}$ (10^{-6} N m^{-1} s)	η_{ef} (Pa s)	$v^* \leftrightarrow v^*_{w/oHI}$ (10^{-25} s^{-1})	CPM (–)	Bead density (10^{22} m^{-3})	h^* (–)
A	3.34 ↔ 4.31	26.72	228.39 ↔ 249.42	4.9	9.92	0.148
B	6.22 ↔ 7.95	48.23	29.37 ↔ 35.48	4.6	3.73	0.149

The subscript "w/oHI" refers to cases without hydrodynamic interaction forces. The acronym CPM = $2MM_{pol}/(LM_{mon})$ means chains per macromolecule (M_{mon} is the molecular weight of the monomer).

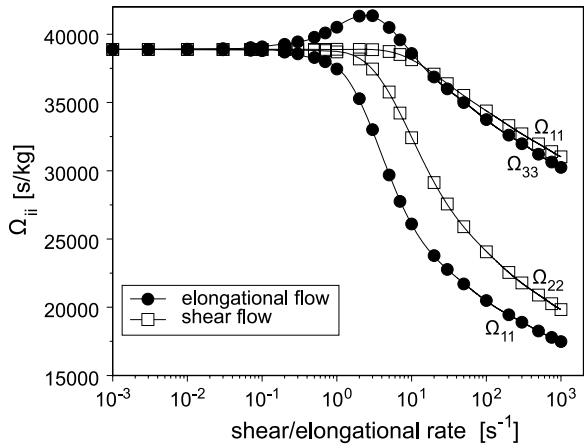

Fig. 2. Comparison between the components Ω_{11}, Ω_{22} and Ω_{33} of the polymer solution A for the cases of simple shear flow and elongational flow.

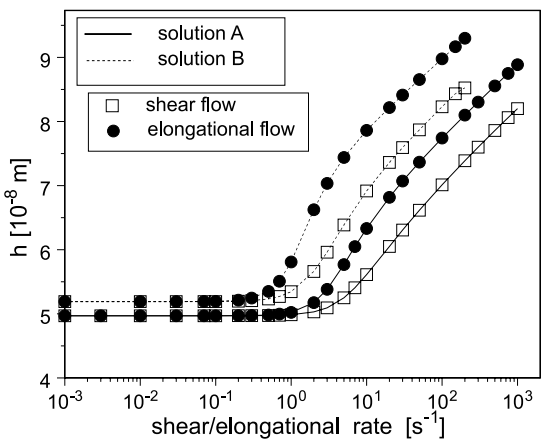

Fig. 3. Mean bead distance h of two arbitrary beads versus the velocity gradient for the cases of simple shear and elongational flow and for the two polystyrene solutions of Table 1.

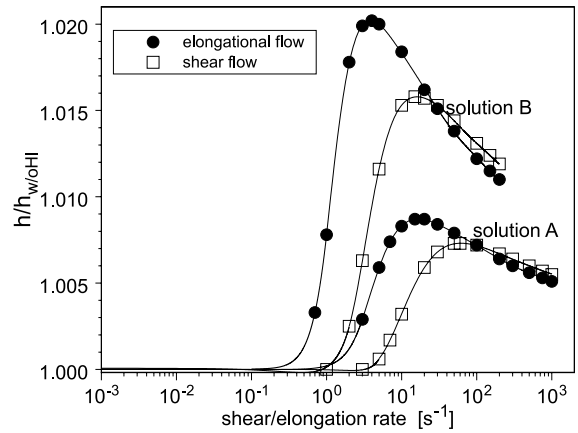

Fig. 4. Ratio $h/h_{w/oHI}$ of the mean bead distance with incorporated hydrodynamic interaction over the mean bead distance without hydrodynamic interaction versus shear and elongation rate. Results for both polystyrene solutions of Table 1 are included.

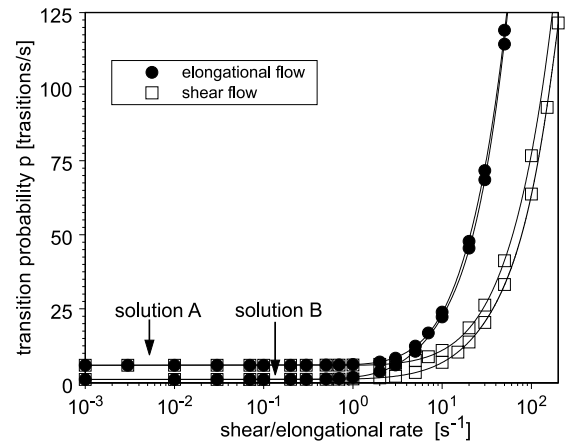

Fig. 5. Transition probability p versus shear and elongation rate for the two solutions of Table 1.

This reduction is exclusively due to the decrease of parameter v^* (Section 4) which dictates the stability of beads. As the velocity gradient increases, the contribution of hydrodynamic interaction gradually gets smaller and practically vanishes for $\dot{\gamma}$ or $\dot{\varepsilon} > 1000\ s^{-1}$. This decay is more intense and shows up at lower velocity gradients in the case of elongational flow than shear flow.

4.2. Viscometric functions

4.2.1. Shear flow

Fig. 7a and b display the dependence of viscometric functions η, Ψ_1 and Ψ_2 on shear rate for both polymer solutions of Table 1, after incorporating the hydrodynamic interaction. For comparison, the experimentally determined values for η and Ψ_1 [22,37] are also shown. A new element compared to earlier predictions of molecular statistical theory of temporary polymer networks which did not account for hydrodynamic interaction [27,29,37] is the non-zero value of viscometric function Ψ_2 (for the improvements regarding the predicted η and Ψ_1 values see later, e.g. Fig. 9). As can be seen, function Ψ_2 is negative throughout the whole examined range of shear rate, taking absolute values much less than the function Ψ_1. In addition, it exhibits a shear thinning behavior over several decades of shear rate, similar to that of η and Ψ_1. The negative sign is in

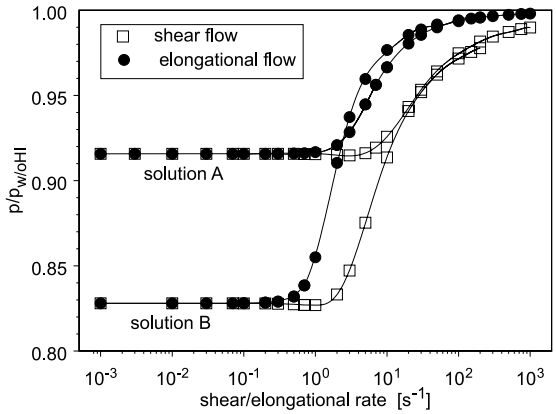

Fig. 6. Ratio $p/p_{w/oHI}$ of the transition probability p with incorporated hydrodynamic interaction over the mean bead distance without hydrodynamic interaction versus shear and elongation rate for the two solutions of Table 1.

agreement with experimental measurements for various solutions [41–43] and it has been predicted by other theories, too [39,44–46].

The zero shear rate value $|\Psi_{20}| = |\lim_{\dot\gamma\to 0}\Psi_2|$ is 1.01% and 1.35% of the value of viscometric function Ψ_1 for solution A and B, respectively (Fig. 8). In the same plot, it is apparent that the ratio Ψ_2/Ψ_1 remains virtually constant up to $\dot\gamma = 0.5\ s^{-1}$ and $0.1\ s^{-1}$, but for larger $\dot\gamma$ it steeply drops and becomes practically zero for $\dot\gamma > 200\ s^{-1}$ and $500\ s^{-1}$, for the two solutions, respectively. The shear-thinning behaviour of the ratio Ψ_2/Ψ_1 for concentrated entangled and semi-dilute entangled polystyrene solutions has been also confirmed experimentally [43].

The influence of hydrodynamic interaction over the other two viscometric functions η and Ψ_1 is shown in Fig. 9. The plot displays the relative percentage variation of these functions, $\Delta\eta_{rel} = (\eta - \eta_{w/oHI})/\eta_{w/oHI}\times 100$ and $\Delta\Psi_{1rel} = (\Psi_1 - \Psi_{1w/oHI})/\Psi_{1w/oHI}\times 100$ versus the shear rate $\dot\gamma$. For $\dot\gamma < 0.3\ s^{-1}$ and $0.1\ s^{-1}$, for solution A and B, respectively, $\Delta\eta_{rel}\kappa\alpha\iota\Delta\Psi_{1rel}$ are negligible. For higher $\dot\gamma$, both functions ascend rapidly until they reach a peak value, whereafter they gradually descend. Regarding differences between polymer solutions A and B, Fig. 9 shows that hydrodynamic interaction comes into play at lower shear rates and is more intense for solution B. The first reflects the corresponding behavior of Ω_{12} whereas the second denotes the greater stability of the beads of solution B (as already argued in Section 4.1).

Evidently, the incorporation of hydrodynamic interaction forces in the so-called non Newtonian

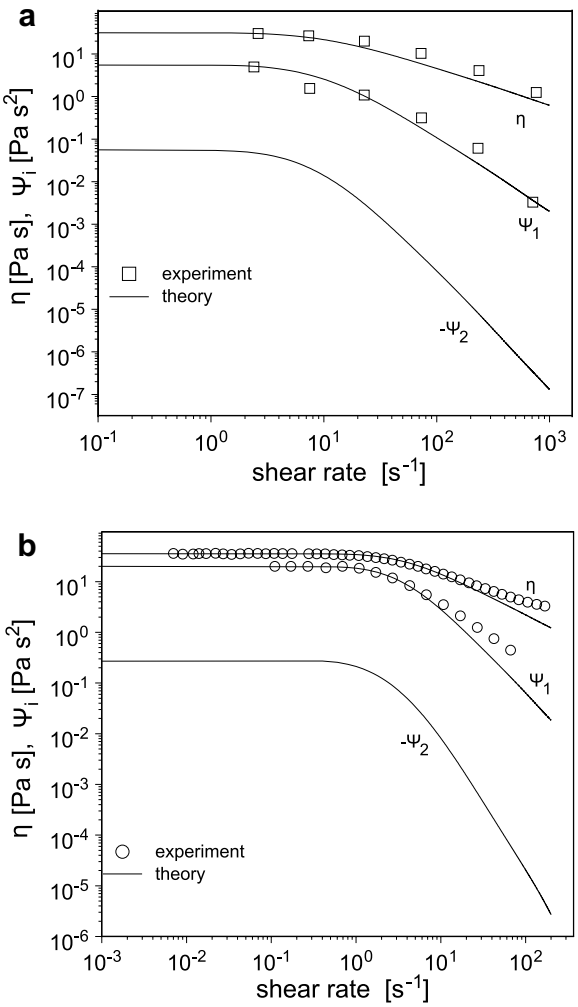

Fig. 7. Dependence of viscometric functions η,Ψ_1 and Ψ_2 on shear rate: (a) for solution A of Table 1, and (b) for solution B of Table 1.

range acts to improve by a small amount the agreement of predictions with experimental measurements. It must be added that the small percentage increase in the predicted values of η and Ψ_1 (Fig. 9) gets actually higher if one takes into account the significant variation in the parameters ζ and v^* after the incorporation of hydrodynamic interaction (as noted in Section 4). The values of these parameters – either before or after accounting for hydrodynamic interaction – are calculated from experimental measurements in such way to correctly reproduce the limiting values $\eta_0 = \lim_{\dot\gamma\to 0}\eta$ and $\Psi_{10} = \lim_{\dot\gamma\to 0}\Psi_1$ for shear flow (see Appendix A). As a result, the old theory in the absence of explicit hydrodynamic interaction terms in Langevin Eq. (2) includes any possible contribution of hydrodynamic

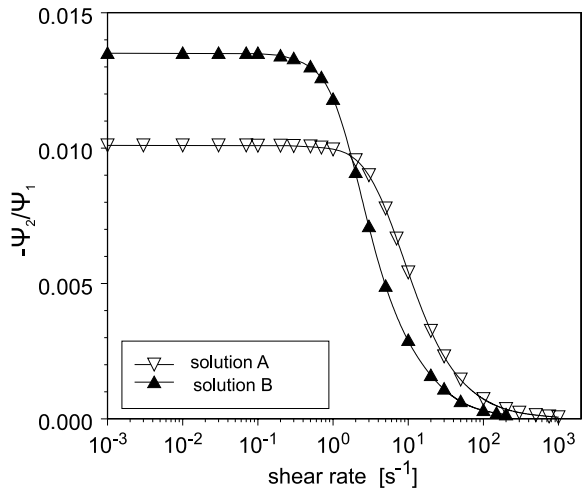

Fig. 8. Ratio of the viscometric function Ψ_2 to the viscometric function Ψ_1 versus shear rate for the two solutions of Table 1.

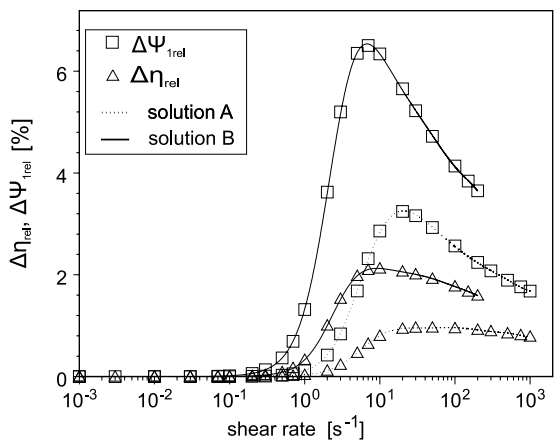

Fig. 9. Relative percentage variation $\Delta\eta_{rel} = (\eta - \eta_{w/oHI})/\eta_{w/oHI}$, $\Delta\Psi_{1rel} = (\Delta\Psi_1 - \Delta\Psi_{1w/oHI})/\Delta\Psi_{1w/oHI}$ of viscometric functions η and Ψ_1 versus shear rate for the two solutions of Table 1. Subscript "w/oHI" refers to the case without hydrodynamic interaction.

interaction in these two parameters by predicting (erroneously) increased friction and instability of the beads. This is readily observed if one uses the values of ζ and v^* obtained after the incorporation of hydrodynamic interaction for the estimation of $\eta_{w/oHI}$ and $\Psi_{1w/oHI}$. Fig. 10 indeed shows (only for solution B but it is similar for solution A) that the deviation between the predictions of the old and the new version of the theory is higher than in Fig. 9. For $\dot{\gamma} < 0.3\ s^{-1}$ this deviation is maximum (9.1% and 14.1% for $\Delta\eta_{rel}$ and $\Delta\Psi_{1rel}$ respectively) whereas it practically vanishes for $\dot{\gamma} > 10\ s^{-1}$. This

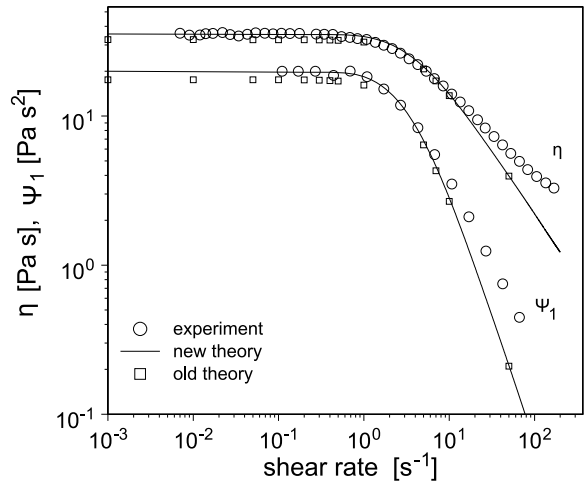

Fig. 10. Comparison between the viscometric functions η, Ψ_1 (for solution B of Table 1) of the old and the new versions of the theory. Calculations are based on the new values of parameters ζ and v^* which account also for hydrodynamic interactions.

behavior manifests that hydrodynamic interaction decreases as bead distance increases (see Fig. 3). Apparently, incorporating these forces leads to higher predicted values for η and Ψ_1.

Nevertheless, what is of greater significance than the slightly better agreement between predictions and measurements is the indication that for semi-dilute polymer solutions hydrodynamic interaction forces may play a role, at least under certain conditions, and so they should not be thoughtlessly neglected as is the tradition for concentrated solutions.

4.2.2. Elongational flow

Fig. 11 presents the variation of elongational viscosity η_e with respect to elongational rate for both polymer solutions A and B, as predicted after incorporating the hydrodynamic interaction in the theory. Clearly, for low elongational rates the value of elongational viscosity is equal to the Trouton viscosity, $3\eta_0$, where $\eta_0 = \lim_{\dot{\gamma}\to 0}\eta$. This stability of the elongational viscosity η_e implies that in this region the stress π^{33}–π^{11} grows proportionally with the elongational rate $\dot{\varepsilon}$. Unfortunately, there are no experimental data available for the particular polystyrene solutions to compare with. Nevertheless, measurements for a similar polystyrene solution with 6.6 CPM (instead of 4.9 and 4.6 of solutions A and B, respectively) display a similar behavior [47] For higher elongational rates, η_e ascends a little

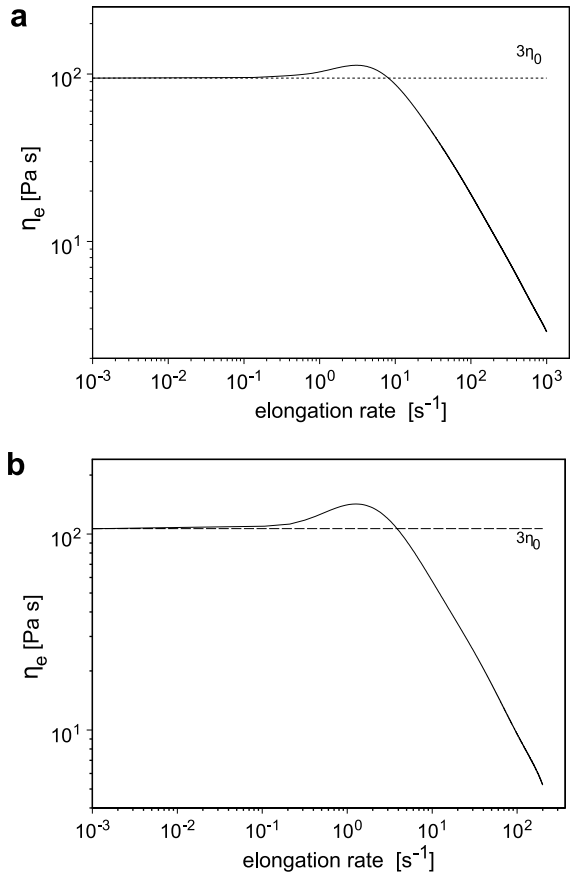

Fig. 11. Dependence of elongational viscosity η_e, on elongational rate: (a) for solution A of Table 1, and (b) for solution B of Table 1.

and becomes maximum at $\dot{\varepsilon} = 3\ s^{-1}$ and $1\ s^{-1}$, for the two polymer solutions, respectively. These peak values are 20% and 34% of η_0, respectively. This increase is attributed to chain stretching and has been also observed in the polystyrene solution of [47] (their Fig. 9). Yet, in the latter study the increase is much higher probably because their solution has a zero shear viscosity ~17–19 times larger than that of our solutions A and B. For even higher elongational rates, the elongational viscosity starts to gradually decrease, intercepting the Trouton viscosity at $\dot{\varepsilon} = 8.3\ s^{-1}$ and $3.8\ s^{-1}$, for solutions A and B, respectively. This decrease seems peculiar if one considers the classical temporary network model with linear springs for which the bead creation and loss rates are independent of the deformation history. The classical model yields an elongation viscosity that goes to infinity at finite elongation rates and steady state shear flow material functions that are independent of the shear rate. But in our approach, the transition probability increases exponentially with the local elastic strain around a junction [18], Fig. 5. As a result, chain stretching and the corresponding stress grow inversely proportional with the elongational rate $\dot{\varepsilon}$. In particular, the mean chain length never exceeds 14% of the maximal possible length regardless how much the elongational rate increases. Therefore, the use of linear springs in our temporary network model does not lead to an infinite stress at high elongation rates. For the same reason the use of linear springs in our model leads to steady state shear flow material functions that depend on shear rate. Apparently, in our approach it is not necessary to replace the Hookean springs by finitely extensile springs to prevent overstretching of the polymer.

Bhattacharjee et al. [47] did not observe a reduction of elongation viscosity with respect to elongation rate like the one shown in Fig. 11. This discrepancy is likely because their measurements were limited to low elongation rates, $\dot{\varepsilon} < 2\ s^{-1}$. On the contrary, a similar reduction with ours has been reported by other authors for dilute polystyrene solutions (in one case even semi-dilute) having much larger molecular weight but with comparable zero shear viscosity with our solutions A and B [48]. Furthermore, a similar qualitative behavior has been predicted for the case of a low-density polyethylene melt by finite elements techniques [49,50] and has been also measured for several entangled polystyrene melts [51].

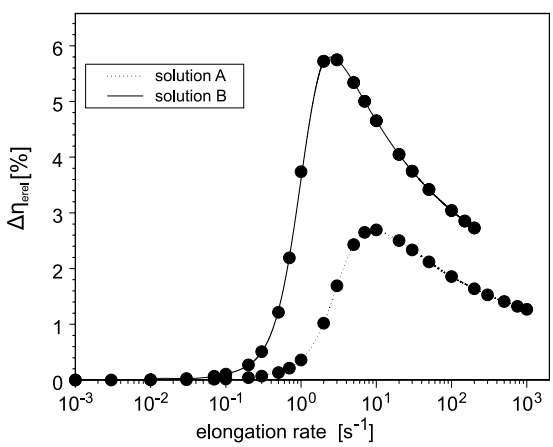

Fig. 12. Relative percentage variation $\Delta\eta_{erel} = (\eta_e - \eta_{ew/oHI})/\eta_{ew/oHI}$ of viscometric function η_e versus elongation rate for the two solutions of Table 1. Subscript "w/oHI" refers to the case without hydrodynamic interaction.

In Fig. 12, one can see that the hydrodynamic interaction force makes the elongational viscosity η_e to take higher values. In particular, for $\dot{\varepsilon} < 0.02\ s^{-1}$ and $0.07\ s^{-1}$ (for solutions A and B respectively), the relative percentage variation $\Delta\eta_{erel} = (\eta_e - \eta_{ew/oHI})/\eta_{ew/oHI} \times 100$ is negligible. Then it acutely rises until it reaches a peak value equal to 2.7% and 5.7% for $\dot{\varepsilon} = 10\ s^{-1}$ and $3\ s^{-1}$ (for solutions A and B, respectively). For even higher velocity gradients, $\Delta\eta_{erel}$ reduces considerably but gradually.

In the case of polymer solution B, the influence of hydrodynamic interaction starts to play a role at lower shear rates and is more intense than in the case of polymer solution A. The first feature reflects the respective behavior of Ω_{33} whereas the second the greater stability of beads in solution B, as already explained in Section 4.1.

5. Conclusions

The present study copes with the incorporation of the hydrodynamic interaction force into the molecular statistical theory of temporary polymer networks, an addition which appears to deserve more attention regarding the quantitative description of the complex behavior of semi-dilute polymer solutions [27–30]. For this, the response of a Langevin-type diffusion equation, accounting also for hydrodynamic interaction, was examined parametrically with the aid of the Oseen tensor. The solution of the diffusion equation for the cases of simple shear and elongational flow leads to the estimation of the respective second moments and, consequently, the stress tensor and viscometric functions η, Ψ_1, Ψ_2 and η_e. Apart from the increase in the predicted values of η and Ψ_1 in the so-called non-Newtonian range which improves a little their agreement with experimental measurements, one should also note the prediction of non-zero values of Ψ_2. Moreover, the predicted negative sign of Ψ_2 is in agreement to experimental measurements for various solutions [41–43].

Acknowledgement

This work has been supported by the Research Committee of Technological Education Institute of Serres.

Appendix A. The transition probability

According to Kroener and Takserman-Krozer 1984 [18], the transition probability is given by the equation

$$\bar{p}(\langle\vec{R}\rangle_R, Z) = \sum_i^M B_i \exp\left[\frac{1}{k_B T}\sum_{i'}^M\sum_j^M k_{ij}(q_{ii'} - q_{ji'})^2\langle(s_{i'})^2\rangle_S\right] \tag{A.1}$$

where

$$B_i \equiv v^*\left(\frac{k_B T}{\alpha^*}\right)^3 (z_{ia} + z_{ib})^{\frac{5}{2}}(z_{ic} + z_{id})^{\frac{5}{2}} \tag{A.2}$$

with

$$\alpha^* = 3k_B T\frac{1}{\sigma}\frac{1-\cos\psi}{1+\cos\psi} \tag{A.3}$$

ψ is the bond angle and σ the structure factor of Volkenstein's statistics [35], both being parameters known for many polymers. Also, z_{ia} through z_{id} are the number of monomers of the four chains forming the junction i. Their values follow from the statistics. This is described in detail in Kroener and Takserman-Krozer 1984 [18] and Chassapis 1986 [27]. Moreover, v^* has the dimension of frequency and is taken from the experiment together with the friction constant ζ and the monomer number L. This is done by comparison with the material parameters $\eta_0 = \lim_{\dot{\gamma}\to 0}\eta$ and $\Psi_{10} = \lim_{\dot{\gamma}\to 0}\Psi_1$ for shear flow. For details see Chassapis [27, Sections 9 and 10], keeping in mind that after the incorporation of hydrodynamic interaction, the respective equations change to:

$$\eta_0 = \eta_S + \frac{N_A c}{LM_{mon}}\frac{k_B T}{2}\sum_{i'}^M \frac{1}{\frac{p_{eq}}{2} + \frac{\lambda_{i'}}{\zeta} + A_{i'}},$$

$$\Psi_{10} = \frac{N_A c}{LM_{mon}}\frac{k_B T}{2}\sum_{i'}^M \frac{1}{\left(\frac{p_{eq}}{2} + \frac{\lambda_{i'}}{\zeta} + A_{i'}\right)^2} \tag{A.4}$$

Appendix B. The factor $(-1)^{(1-\delta_{kl})}$

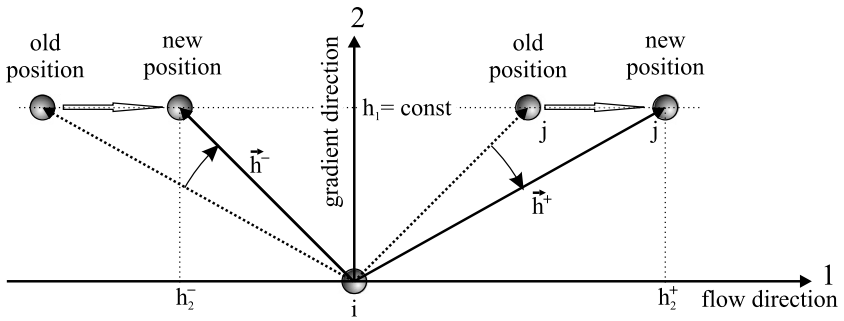

Let us consider two arbitrary beads i and j for the case of simple shear flow with j being located in the upper semi-infinite space of i, i.e. on the 1st or 2nd quadrant, respectively (see at the schematic above). The corresponding average vectors $\langle\vec{h}_{ij}\rangle$ are denoted as $\vec{h}^{+}$ and $\vec{h}^{-}$, because the Ω^{12} component of the Oseen tensor $\underline{\underline{\Omega}}_{ij}(\vec{h}^{+/-})$ is positive or negative accordingly:

$$\Omega^{12+} \sim \frac{h_1^+ h_2^+}{(h^+)^3} > 0, \quad \Omega^{12-} \sim \frac{h_1^- h_2^-}{(h^+)^3} < 0,$$
$$\text{with } h^{+/-} = \sqrt{(h_1^{+/-})^2 + (h_2^{+/-})^2} \tag{B.1}$$

Furthermore, in accordance with the findings of the molecular statistical theory of temporary polymer networks [18,27–30], the following relations hold:

$$\langle\vec{h}_{ij}\vec{h}_{ij}\rangle = \sum_{i'=1}^{M}(q_{ji'} - q_{ii'})^2\langle\vec{s}_{i'}\vec{s}_{i'}\rangle \quad (q_{ii'} = \text{const.})$$
$$\langle\vec{s}_{i'}\vec{s}_{i'}\rangle^{11} = \langle\vec{s}_{i'}\vec{s}_{i'}\rangle^{33} = \langle\vec{s}_{i'}\vec{s}_{i'}\rangle^{22}_{\text{eq}} = \frac{k_B T}{\lambda_{i'}} = \text{const.}$$
$$\langle\vec{s}_{i'}\vec{s}_{i'}\rangle^{22} \geqslant \langle\vec{s}_{i'}\vec{s}_{i'}\rangle^{22}_{\text{eq}}$$
$$\langle\vec{s}_{i'}\vec{s}_{i'}\rangle^{12} = \langle\vec{s}_{i'}\vec{s}_{i'}\rangle^{21} \geqslant 0$$
(equality holds in equilibrium) (B.2)

Combining relations (B.2) and (B.1) yields the following qualitative model of the average behavior of the aforementioned system of two beads:

In equilibrium $(\dot{\gamma} = 0)$ it is $h_1^+ = h_1^- = h_2^+ = h_2^-$ due to the isotropy of the network and so $\Omega_{\text{eq}}^{12+} = -\Omega_{\text{eq}}^{12-}$. Consequently, the mean value $\Omega_{\text{eq}}^{12} = \frac{1}{2}(\Omega_{\text{eq}}^{12+} + \Omega_{\text{eq}}^{12-})$ is equal to zero. As shear rate increases $(\dot{\gamma} > 0), h_2^+$ increases and h_2^- decreases because of the orientation of the network chains, whereas h_1 stays unchanged on account of the stability of $\langle\vec{s}_{i'}\vec{s}_{i'}\rangle^{11}$. This results in higher absolute values of Ω^{12-} and lower values of Ω^{12+}. Thus, the mean value $\Omega^{12} = \frac{1}{2}(\Omega^{12+} + \Omega^{12-})$ is negative.

In the present case since we do not know the average vectors $\vec{h}^{+}$ and $\vec{h}^{-}$ for each separate quadrant, we can use their composite resultant $\vec{h}$, in a manner similar with the substitution of $\underline{\underline{\Omega}}_{ij}(\vec{R})$ by $\underline{\underline{\Omega}}_{ij}(\langle\vec{R}\rangle)$, and then the following qualitative model emerges:

In an equilibrium state $(\dot{\gamma} = 0)$, $h_2 = 0$ because of the network isotropy. This yields that the mean value $\Omega_{\text{eq}}^{12} \sim h_2$ equals to zero. With increasing shear rate $(\dot{\gamma} > 0)$, the average vector $\vec{h}$ rotates in the 1st quadrant due to orientation of the network chains and makes h_2, to rise while h_1 remains unchanged dictated by the stability of $\langle\vec{s}_{i'}\vec{s}_{i'}\rangle^{11}$. As a consequence, $\Omega^{12} \sim h_2$ increases and becomes positive, i.e., contrary to the more accurate description above Analogous is the situation when the bead j is located in the lower semi-infinite space of i.

From the above, it is evident that the factor $(-1)^{(1-\delta_{kl})}$ in Eq. (10) acts to restore the correct sign in the approximation $\underline{\underline{\Omega}}_{ij}(\vec{R}) \to \underline{\underline{\Omega}}_{ij}(\langle\vec{R}\rangle)$ whereas the absolute value of the non-vanishing non-diagonal Oseen tensor components remains unaffected.

References

[1] De Gennes PG. Reptation of a polymer chain in the presence of fixed obstacles. J Chem Phys 1971;55:572–9.
[2] Doi M, Edwards SF. Dynamics of concentrated polymer systems. Part 1: Brownian motion in the equilibrium state. J Chem Soc Faraday Trans II 1978;74:1789–801.
[3] Doi M. Explanation of the 3.4-power law for viscosity of polymeric liquids on the basis of the tube model. J Polym Sci Polym Phys Ed 1983;21:667–84.
[4] Ketzmerick R, Öttinger HC. Simulation of a non-Markovian process modeling contour length fluctuations in the Doi–Edward model. Continuum Mech Thermodyn 1989;1:113.

[5] Milner ST, McLeish TCB. Reptation and contour-length fluctuations in melts of linear polymers. Phys Rev Lett 1998; 81(3):725–8.
[6] Marrucci G, Grizzuti N. Fast flows of concentrated polymers – predictions of the tube model on chain stretching. Gazz Chim Ital 1988;118:179–85.
[7] Mead DW, Leal LG. The reptation model with segmental strech. I Basic equations and general properties. Rheol Acta 1995;34:339–59.
[8] Mead DW, Larson RG, Doi M. A molecular theory for fast flows of entangled polymers. Macromolecules 1998;31: 7895–914.
[9] Marrucci G, Ianniruberto G. Flow-induced orientation and stretching of entangled polymers. Philos Trans R Soc Lond 2003;A361:677–87.
[10] Tsenoglou C. Viscoelasticity of binary homopolymer blends. ACS Polym Preprints 1987;28:185–6.
[11] Des Cloiseaux J. Double reptation vs. simple reptation in polymer melts. Europhys Lett 1988;5:437–42.
[12] Öttinger HC. Modified reptation model. Phys Rev 1994;E50: 4891–5.
[13] Marrucci G. Dynamics of entanglements: a nonlinear model consistent with the Cox-Merz rule. J Non-Newtonian Fluid Mech 1996;62:279–89.
[14] Ianniruberto G, Marrucci G. On compatibility of the Cox-Merz rule with the model of Doi and Edwards. J Non-Newtonian Fluid Mech 1996;65:241–6.
[15] Fang J, Losinski A, Owens RG. Towards more realistic kinetic models for concentrated solutions and melts. J Non-Newtonian Fluid Mech 2004;122:79–90.
[16] Watanabe H. Viscoelasticity and dynamics of entangled polymers. Prog Polym Sci 1999;24:1253–403.
[17] Altukhov YuA, Pokrovskii VN, Pyshnograi GV. On the difference between weakly and strongly entangled linear polymers. J Non-Newtonian Fluid Mech 2004;121:73–86.
[18] Kroener E, Takserman-Krozer. Statistical mechanics of temporary polymer networks. Rheol Acta 1984;23:1–9. and 139–50.
[19] Bird BR, Hassager O, Armstrong RC, Curtis CHF. Dynamic of polymeric liquids, vol. 2. New York: Wiley; 1987.
[20] Giesekus H. A simple constitutive equation for polymer fluids based on the concept of the deformation dependent tensorial mobility. J Non-Newtonean Fluid Mech 1982;11: 69–109.
[21] Phan-Thien N, Tanner RI. A new constitutive equation derived from network theory. J Non-Newtonean Fluid Mech 1977;2:353–65.
[22] Li JM, Burghardt W, Yang B, Khomami B. Flow birefringence and computational studies of a shear thinning polymer solution in axisymmetric stagnation flow. J Non-Newtonean Fluid Mech 1998;74:151–94.
[23] Verbeeten WMH, Petres GWM, Baaijens FPT. Viscoelastic analysis of complex polymer melt flows using the eXtended Pom-Pom model. J Non-Newtonean Fluid Mech 2002;108: 301–26.
[24] Quinzani LM, Armstrong RC, Brown RA. Birefringence and Laser-Doppler velocimetry (LDV) studies of viscoelastic flow through a planar contraction. J Non-Newtonean Fluid Mech 1994;52:1–36.
[25] Baaijens FPT, Baaijens HPW, Peters GWM, Meijer HEH. An experimental and numerical investigation of a viscoelastic flow around a cylinder. J Rheol 1994;38:351–76.
[26] Baaijens HPW, Peters GWM, Baaijens FTP, Meijer HEH. Viscoelastic flow past a confined cylinder of a polyisobutylene solution. J Rheol 1995;39:1243–77.
[27] Chassapis D. Zur molekular-statistischen Theorie temporaerer Plolymernetzwerke – Theoretische Untersuchungen und Vergleich mit Experimenten. PhD dissertation, University of Stuttgart, 1986.
[28] Kroener E, Chassapis D, Takserman-Krozer R. The physics of temporary polymer networks. In: Kramer O, editor. Biological and synthetic polymer networks. London: Elsevier; 1988. p. 185–205.
[29] Chassapis D, Babos G, Takserman-Krozer R, Kroener E. Statistical mechanics of temporary polymer networks, dynamical effects. Rheol Acta 1989;28:193–201.
[30] Chassapis D, Balouktsis A, Karapantsios TD. Flow birefringence of temporary polymer networks. Eur Pol J 2002; 38:1071–8.
[31] De Gennes PG. Scaling concepts in polymer physics. Ithaca: Cornell University Press; 1979.
[32] Larson RG. Constitutive equations for polymer melts and solutions, Series in chemical engineering. Boston: Butterworth; 1988.
[33] Rouse PE. A theory of the linear viscoelastic properties of dilute solutions of coiling polymers. J Chem Phys 1953;21: 1272–80.
[34] Zimm BH. Dynamics of polymer molecules in dilute solution: viscoelasticity, flow birefringence and dielectric loss. J Chem Phys 1956;24:269–81.
[35] Volkenstein MV. In: Configurational statistics of polymer chains. New York: Interscience; 1963.
[36] Flory P. Statistical mechanics of chain molecules. New York: Interscience; 1969.
[37] Krozer S, Tawadjoh M, Gruber E. Zur Beschreibung der rheologischen Eigenschaften konzentrierter Polystyrol-Lösungen. Rheol Acta 1977;16:438–43.
[38] Johnson RM, Schrag JL, Ferry JD. Infinite-dilution viscoelastic properties of polystyrene in Θ-solvents and good solvents. Polym J 1970;1:742–9.
[39] Prakash JR, Öttinger HC. Universal viscometric functions for dilute polymer solutions. J. Non-Newtonean Fluid Mech 1997;71:245–72.
[40] Chih-Chen Hsieh, Lei Li, Ronald G. Larson. Modeling hydrodynamic interaction in Brownian dynamics: simulations of extensional flows of dilute solutions of DNA and polystyrene. J Non-Newtonean Fluid Mech 2003;113: 147–91.
[41] Christiansen EB, Leppard WR. Steady-state and oscillatory flow properties of polymer solutions. Trans Soc Rheol 1974;18:65–86.
[42] Magda JJ, Lee CS, Muller SG, Larson RG. Rheology, flow instabilities, and shear-induced diffusion in polystyrene solutions. Macromolecules 1993;26:1696–706.
[43] Magda JJ, Baeck SG. Concentrated entangled and semidilute entangled polystyrene solutions and the second normal stress difference. Polymer 1994;35:1187–94.
[44] Petera D, Muthukumar M. Brownian dynamics simulation of bead-rod chains under shear with hydrodynamic interaction. J Chem Phys 1999;111:7614–23.
[45] Chih-Chen Hsieh, Larson RG. Modeling hydrodynamic interaction in Brownian dynamics: simulations of exyensional and shear flows of dilute solutions of high molecular weight polystyrene. J Rheol 2004;48:995–1021.

[46] Liu S, Ashok B, Muthukumar M. Brownian dynamics simulations of bead-rod-chain in simple shear flow and elongational flow. Polymer 2004;45:1383–9.
[47] Bhattacharjee PK, Oberhauser JP, Mckinley GH, Leal LG, Sridhar T. Extensional rheometry of entangled solutions. Macromolecules 2002;35:10131–48.
[48] Gupta RK, Nguyen DA, Sridhar T. Extensional viscosity of dilute polystyrene solutions: effect of concentration and molecular weight. Phys. Fluids 2000;12:1296–318.
[49] Feigl K, Tanner FX, Edwards BJ, Collier JR. A numerical study of the measurement of elongational viscosity of polymeric fluids in a semihyperbolically converging die. J Non-Newtonean Fluid Mech 1987;26:207–46.
[50] McLeish TCB, Larson RG. Molecular constitutive equations for a class of branched polymers: the Pom-Pom polymer. J Rheol 1998;42:81–110.
[51] Nielsen JK, Rasmussen HK, Hassager O, McKinley GH. Elongational viscosity of monodisperse and bidisperse polystyrene melts. J Rheol 2006;50(4):453–76.